Outage Analysis of Alamouti-NOMA Scheme for Hybrid Satellite–Terrestrial Relay Networks

Mesut Toka, *Member, IEEE*, Mojtaba Vaezi, *Senior Member, IEEE*, and Wonjae Shin, *Senior Member, IEEE*

***Abstract*—In this article, we investigate the performance of hybrid satellite–terrestrial relay networks with multiuser downlink nonorthogonal multiple access. The satellite applies Alamouti space–time block coding, and users exploit a receive antenna selection technique. Communication between the satellite and users is assumed to be established with the aid of a half-duplex terrestrial relay equipped with multiple receive antennas and operating in amplify-and-forward mode, because of the heavy masking effects attributed to environmental obstacles. Subsequently, the satellite–relay link is exposed to shadowed-Rician fading, whereas the relay–users links undergo Nakagami-*m* fading, which is a generic statistical channel model for nonterrestrial networks. To be more practical, we consider imperfect successive interference cancellation. The exact outage probability of each user and the corresponding asymptotic expression at the high signal-to-noise ratio are derived to demonstrate the system performance. The analysis indicates that the shadowing conditions do not affect the array gain when the diversity order is dominated by the multiantenna configuration of the second hop. The theoretical derivations are validated by using Monte Carlo simulations. The numerical results indicate that the proposed scheme significantly improves the performance of each user under various shadowing conditions. It also outperforms orthogonal multiple access when proper power levels are allocated to users.**

***Index Terms*—Alamouti code, antenna selection, hybrid satellite–terrestrial relay network (HSTRN), nonorthogonal multiple access (NOMA), relay, satellite communication.**

I. Introduction

THE EXPLOITATION of satellites in wireless communications, such as fifth-generation (5G) and beyond cellular networks, has attracted considerable interest over the last decade for overcoming the limitations of the existing ground base stations (BSs) in terms of coverage area, data rates, and service continuity. Satellites are considered a promising solution to satisfy the requirements of the rapidly increasing smart devices such as Internet of Things (IoT) networks [1]; this is because such devices are deployed at places where proper service may not be possible via terrestrial networks, e.g., in rural areas and aerial vehicles [1], [2], [3]. However, channel quality in a satellite–terrestrial environment can be poor because of *masking effects* due to the atmosphere, obstacles, and heavy path loss, to the extent that even establishing a proper End-to-End (E2E) communication may be impossible. These masking effects become severer for indoor/outdoor users in an urban area.

To overcome the aforementioned issue, the use of terrestrial nodes as relay assistance in satellite systems, called hybrid satellite–terrestrial relay network (HSTRN), has arisen and attracted considerable research interest [4], [5]. Within this context, many studies have focused on demonstrating the superiority of HSTRN by considering single-antenna [6], [7] and multiple-antenna techniques [8], [9], [10], [11]. In the scope of satellite–terrestrial networks, traditional orthogonal multiple access (OMA) schemes, such as time division, frequency division, and code division, have been extensively investigated. However, when serving massive IoT devices within a vast territory based on multiple beams, OMA techniques can suffer from significant scheduling delays, large spectrum requirements, and severe multiple-access interference [12], [13]. The nonorthogonal multiple access (NOMA) scheme has recently gained interest in the context of satellite–terrestrial networks to overcome the above-mentioned limitations of OMA. NOMA enables multiple users to share the same resource in a nonorthogonal manner, and this ensures high spectral efficiency and low latency while providing a good balance between throughput and user fairness [14], [15], [16].

The performance of NOMA without relaying/cooperation was investigated for satellite networks in [17], [18], and [19]. In addition, NOMA-based HSTRNs were studied in [20], [21], [22], [23], [24], and [25]. Yan et al. [20] analyzed the outage probability (OP) and ergodic capacity (EC) of an HSTRN for a two-user NOMA scheme, wherein a strong user behaves as a decode-and-forward (DF) relay and assists a weak user. The authors derived exact OP and EC expressions by considering the maximal-ratio combining (MRC) at the weak user to combine direct and relayed signals. Xie et al. [21] addressed power allocation optimization based on the derived OP expression for HSTRNs with multiuser NOMA by considering DF/amplify-and-forward (AF) relaying to ensure fairness among users, and they developed a low-complexity algorithm. Singh and Upadhyay [22] investigated cooperative NOMA-based cognitive satellite networks, wherein secondary

Manuscript received 26 July 2022; revised 27 September 2022; accepted 10 November 2022. Date of publication 15 November 2022; date of current version 7 March 2023. This work was supported in part by the Institute of Information and Communications Technology Planning and Evaluation under Grant 2022-0-00704, Grant 2021-0-00260, and Grant 2018-0-01424; and in part by the Basic Science Research Programs under the National Research Foundation of Korea (NRF) funded by the Ministry of Science and ICT under Grant 2022R1A2C4002065 and Grant 2021R1A4A1030775. *(Corresponding author: Wonjae Shin.)*

Mesut Toka and Wonjae Shin are with the Department of Electrical and Computer Engineering, Ajou University, Suwon 16499, South Korea (e-mail: tokamesut@ajou.ac.kr; wjshin@ajou.ac.kr).

Mojtaba Vaezi is with the Department of Electrical and Computer Engineering, Villanova University, Villanova, PA 19085 USA (e-mail: mvaezi@villanova.edu).

Digital Object Identifier 10.1109/JIOT.2022.3222414

2327-4662 © 2022 IEEE. Personal use is permitted, but republication/redistribution requires IEEE permission.
See https://www.ieee.org/publications/rights/index.html for more information.

Authorized licensed use limited to: VILLANOVA UNIVERSITY. Downloaded on September 28,2023 at 20:22:30 UTC from IEEE Xplore. Restrictions apply.

and primary communications comprise terrestrial and satellite concepts, respectively. In the secondary transmission, a stronger NOMA user acts as a full-duplex DF relay, and all secondary users suffer from interference caused by satellite transmission. In [23], a regenerative satellite-assisted cooperative two-user NOMA system was considered. The authors applied a coordinated direct and relayed transmission scheme, wherein the weak user requires assistance from the satellite while the strong user enjoys the service of both the BS and satellite. The exact OP expressions were derived as performance measures.

However, the above-mentioned studies focused only on single-antenna cases. To exploit the benefits of multiple-antenna schemes, Yan et al. [24] considered MRC for users in a multiuser NOMA-based HSTRN, and they derived the exact OP expressions. It has been shown that the performance can be improved in terms of coding gain; however, it is limited to the diversity order by increasing the number of antennas. Considering the same system used in [24], the MRC and maximal-ratio transmission were applied at the terrestrial relay node to jointly exploit the benefits of receive and transmit diversities in [25]. Furthermore, the exact OP expressions were derived by considering the effects of rain attenuation. However, the authors considered that the satellite and users are equipped with a single antenna.

A. Motivations and Contributions

Multiple-antenna techniques improve the throughput and diversity gain of terrestrial systems. However, considering multiple-antenna techniques in satellite networks is challenging because the absence of scattering around the satellite prevents the benefits of multipath fading, as explained in [26]. On the other hand, because of the fast-varying nature and significant propagation delay caused by long distances in the satellite–terrestrial environment, it is well known in the literature that obtaining perfect channel state information (CSI) is difficult. Thus, Arti and Jindal [26], Ruan et al. [27], and Zhao et al. [28] considered using a space–time block coding (STBC) scheme, i.e., the Alamouti code [29], in OMA-based satellite–terrestrial networks; this is because it does not require CSI to achieve transmit diversity. In this article, we focus on investigating the Alamouti code and receive antenna selection (RAS) at the satellite and users, respectively, in a multiuser NOMA-based HSTRN.[1] The main contributions of this article are summarized as follows.

1) We exploit the Alamouti code at the satellite node in a multiuser NOMA-based HSTRN to overcome the CSI burden in the satellite link while retaining the benefits of spatial diversity. In addition, the terrestrial relay is considered to employ multiple receive antennas to increase the received signal strength.
2) Furthermore, the RAS scheme is applied at the user nodes since it requires only partial CSI and reduces hardware complexity owing to deployment of a single radio-frequency (RF) chain together with increased receiver diversity, which is well suited for IoT devices. Moreover, imperfect successive interference cancellation (SIC) is considered in the analysis to improve the practicality of the considered system.
3) We derive exact closed-form OP expressions for all users to demonstrate the performance behavior. In addition, we obtain the asymptotic OP expressions, i.e., the OP behavior at the high signal-to-noise ratio (SNR) region to provide better insights in terms of diversity order and array gain. Analyses are conducted for shadowed-Rician and Nakagami-m fading for satellite–relay and relay–users links, respectively. Thus, the network considered in this article involves a generic scenario for HSTRN.
4) The accuracy of the theoretical derivations was confirmed using extensive Monte Carlo simulations. Furthermore, comparisons are drawn with the benchmark OMA scheme and the results are presented.

[1]The conference version of this article [30] addresses the two-user scenario and presents only simulations without considering satellite parameters and practical imperfections.

B. Organization and Notations

The remainder of this article is organized as follows. Section II provides a detailed introduction to the system model and channel statistics. In Section III, we derive the exact OP expression for users, with its asymptotic expression. The numerical results are presented in Section IV to validate the theoretical analyses. Finally, Section V presents the conclusions.

Notations: Bold lowercase and uppercase letters represent vectors and matrices, respectively. $\|\cdot\|_{\mathsf{F}}$ denotes the Frobenius norm. $[\,\cdot\,]^{\mathsf{T}}$ and $[\,\cdot\,]^{\mathsf{H}}$ represent the transpose and conjugate transpose of a vector (matrix), respectively, and $(\cdot)^*$ is the conjugate of a complex variable. $\mathcal{CN}(0,\sigma^2)$ represents the complex Gaussian distribution with a zero mean and variance of σ^2. $\mathbb{P}(\cdot)$ denotes the probability of an event, and $f_X(\cdot)$ and $F_X(\cdot)$ indicate the probability density function (PDF) and cumulative distribution function (CDF) of random variable X, respectively. $\mathbb{E}[\,\cdot\,]$ denotes the expectation operator.

II. System Model

Consider a downlink HSTRN based on power-domain NOMA in which the geostationary (GEO) satellite (S) applies the Alamouti STBC scheme to communicate with K terrestrial IoT users (U_k, $1 \le k \le K$), each equipped with N antennas, as shown in Fig. 1. The dedicated terrestrial half-duplex relay (R) is equipped with one transmit antenna and N_{R} receive antennas, and it adopts the AF protocol. At the receiver side, each user exploits the RAS technique for signal reception. Note that the RAS technique reduces hardware complexity by deploying only a single RF chain. We assume that the direct link cannot be established between the satellite and users because of the heavy shadowing or atmospheric fading caused by environmental masking effects.

The satellite generates an Alamouti code matrix as [29]

$$\mathbf{X} = \begin{bmatrix} x_1 & x_2 \\ -x_2^* & x_1^* \end{bmatrix} \tag{1}$$

Authorized licensed use limited to: VILLANOVA UNIVERSITY. Downloaded on September 28,2023 at 20:22:30 UTC from IEEE Xplore. Restrictions apply.

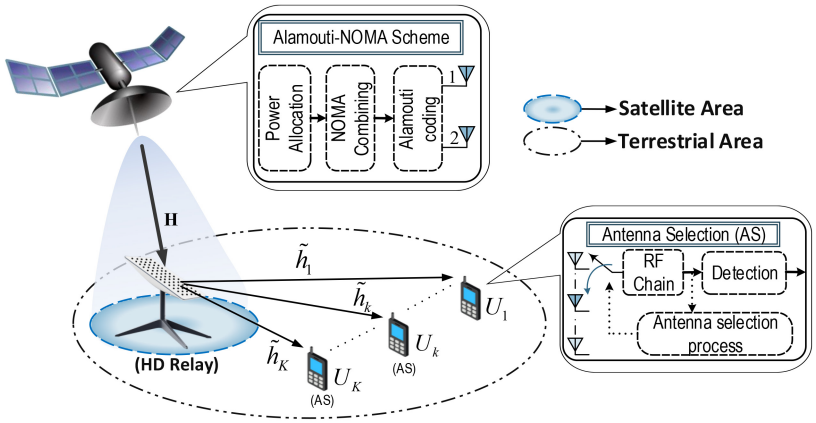

Fig. 1. System model of Alamouti-NOMA-based HSTRN.

whose elements include superimposed symbols related to the users such that

$$x_1 = \sum_{k=1}^{K} \sqrt{a_k P_S/2}\, s_{k1} \quad \text{and} \quad x_2 = \sum_{k=1}^{K} \sqrt{a_k P_S/2}\, s_{k2}$$

because we are considering nonorthogonal transmission. Here, s_{k1} and s_{k2} represent the first and second unit energy symbols of the kth NOMA user, respectively, a_k is the power allocation coefficient for the kth user, and P_S represents the transmit power at the satellite.

Consider the first hop of the transmission (satellite to relay). Let $\mathbf{y}_{R,1}$ ($N_R \times 1$) and $\mathbf{y}_{R,2}$ ($N_R \times 1$) represent signal vectors received by all antennas of the relay in the first and second time intervals according to the Alamouti transmission, respectively, and define $\mathbf{H} = [\mathbf{h}^{(1)}\ \mathbf{h}^{(2)}]^T$ as the channel coefficient matrix of the satellite–relay link, where $\mathbf{h}^{(1)} = [h^{(1,1)}\ h^{(1,2)} \cdots h^{(1,N_R)}]^T$ and $\mathbf{h}^{(2)} = [h^{(2,1)}\ h^{(2,2)} \cdots h^{(2,N_R)}]^T$. Here, $h^{(i,j)}$ represents the channel coefficient between the ith antenna of the satellite and the jth antenna of the relay. Thus, the equivalent received signal matrix at the relay, i.e., $\mathbf{Y}_R = [\mathbf{y}_{R,1}^T\ \mathbf{y}_{R,2}^H]^T$, is expressed as

$$\mathbf{Y}_R = \sqrt{\mathcal{H}}\mathbf{H}_{eq}\mathbf{x} + \mathbf{Z}_R \tag{2}$$

where $\mathbf{Z}_R = [\mathbf{z}_{R,1}^T\ \mathbf{z}_{R,2}^H]^T$ represents the noise matrix at the relay. $\mathbf{z}_{R,1}$ ($N_R \times 1$) and $\mathbf{z}_{R,2}$ ($N_R \times 1$) are noise vectors corresponding to the first and second time intervals at the relay, respectively; each element of the vectors is distributed as $\mathcal{CN}(0, \sigma_R^2)$. $\mathbf{x} = [x_1\ x_2]^T$ denotes the superimposed symbols transmitted within the Alamouti code matrix; the equivalent channel matrix $\mathbf{H}_{eq}$ can be expressed as

$$\mathbf{H}_{eq} = \begin{bmatrix} \mathbf{h}^{(1)} & \mathbf{h}^{(2)} \\ \left(\mathbf{h}^{(2)}\right)^* & -\left(\mathbf{h}^{(1)}\right)^* \end{bmatrix}.$$

Furthermore, $\mathcal{H}$ denotes the unified parameter of RF propagation losses and noise power between the satellite and relay, which can be expressed as [31]

$$\begin{aligned} \mathcal{H}(\text{dB}) = G_S + G_R(\theta) - L_{FSL} - T - \kappa_B \\ - W - L_{SL} - L_{AL} \end{aligned} \tag{3}$$

where G_S and $G_R(\theta)$ represent the antenna gain of the satellite and beam gain of the satellite–relay link, respectively. In addition, L_{FSL} indicates the free-space path loss calculated using $L_{FSL} = 92.44 + 20\log_{10}(f_c) + 20\log_{10}(d)$, where f_c and d denote the carrier frequency (in GHz) and distance (in km) between the satellite and relay, respectively. The remaining loss parameters can be described as follows: κ_B, T, and W denote the Boltzmann constant, noise temperature at relay, and bandwidth, respectively; and L_{SL} and L_{AL} represent the scintillation and atmospheric losses [31], [32]. The approximated beam gain can be obtained as [13]

$$G_R(\theta) = G_{max}\left(\frac{J_1(u)}{2u} + 36\frac{J_3(u)}{u^3}\right)^2$$

where G_{max} represents the maximum beam gain at the relay, and $J_n(\cdot)$ denotes the nth-order first-kind Bessel function [33, eq. (8.402)]. $u = 2.07123\sin(\theta)/\sin(\theta_{3dB})$, where θ represents the angle between the beam center and relay as observed from the satellite, and θ_{3dB} is the one-sided half-power beamwidth.

The signals received by all antennas at the relay are combined, and, therefore, the combination process can be expressed as $\tilde{\mathbf{Y}}_R = \mathbf{H}_{eq}^H\mathbf{Y}_R$. Subsequently, in the second hop, the relay amplifies the received signal by multiplying it by the amplifying factor ϖ. If we limit the power of the signal transmitted by the relay to P_R, we can determine the amplifying factor using (2) as

$$\varpi = \sqrt{P_R/\left(\mathcal{H}P_S\|\mathbf{H}\|_F^2 + \sigma_R^2\right)}. \tag{4}$$

The relay broadcasts the amplified signal to all users, and thus, the received signal vector at the kth user is expressed as

$$\begin{aligned} \mathbf{y}_k &= \varpi\tilde{h}_k\tilde{\mathbf{Y}}_R + \mathbf{n}_k \\ &= \varpi\tilde{h}_k\sqrt{\mathcal{H}}\mathbf{H}_{eq}^H\mathbf{H}_{eq}\mathbf{x} + \varpi\tilde{h}_k\mathbf{H}_{eq}^H\mathbf{Z}_R + \mathbf{n}_k \end{aligned} \tag{5}$$

where $\tilde{h}_k$ denotes the channel coefficient between the relay and the selected antenna for the kth user, and $\mathbf{n}_k = [n_{k,1}\ n_{k,2}]^T$ represents the noise vector with $n_{k,1}, n_{k,2} \sim \mathcal{CN}(0, \sigma_k^2)$. Here, because we apply the RAS scheme to the users, during the training period, the relay sends pilot symbols to all users in turns. Each user then determines the receive antenna providing the highest instantaneous SNR. Consequently, the magnitude-squared function of the channel gain between the relay and the selected antenna is denoted by $|\tilde{h}_k|^2 = \max_{1\le r\le N}\{|h_{k,r}|^2\}$ [34].

Authorized licensed use limited to: VILLANOVA UNIVERSITY. Downloaded on September 28,2023 at 20:22:30 UTC from IEEE Xplore. Restrictions apply.

A. Channel Statistics

1) Satellite Channel Statistics: In the first hop, the PDF of the squared channel gain between the ith antenna of the satellite and the jth antenna of the relay, assuming that channels between the satellite and relay undergo independent and identically distributed (i.i.d.) shadowed-Rician fading,[2] can be expressed as [36]

$$f_{|h^{(i,j)}|^2}(x) = \alpha_{\mathrm{SR}} e^{-\beta_{\mathrm{SR}} x} {}_1F_1(m_{\mathrm{SR}}; 1; \delta_{\mathrm{SR}} x), \quad (x > 0) \tag{6}$$

where $\alpha_{\mathrm{SR}} = (2b_{\mathrm{SR}} m_{\mathrm{SR}}/(2b_{\mathrm{SR}} m_{\mathrm{SR}} + \Omega_{\mathrm{SR}}))^{m_{\mathrm{SR}}}/(2b_{\mathrm{SR}})$, $\beta_{\mathrm{SR}} = 0.5/b_{\mathrm{SR}}$, and $\delta_{\mathrm{SR}} = \Omega_{\mathrm{SR}}/(2b_{\mathrm{SR}}(2b_{\mathrm{SR}} m_{\mathrm{SR}} + \Omega_{\mathrm{SR}}))$. Here, $2b_{\mathrm{SR}}$ denotes the average power of the multipath component, and Ω_{SR} and $m_{\mathrm{SR}} \geq 0$ represent the average powers of the line-of-sight component and Nakagami-m fading parameters, respectively. ${}_1F_1(\cdot;\cdot;\cdot)$ denotes the confluent hypergeometric function of the first kind [33, eq. (9.210.1)]. Note that we consider arbitrary integer values of the fading parameter of m_{SR} throughout this article. Thus, with the aid of the series expansion of ${}_1F_1(\cdot;\cdot;\cdot)$, (6) can be re-expressed as [37]

$$f_{|h^{(i,j)}|^2}(x) = \alpha_{\mathrm{SR}} \sum_{q=0}^{m_{\mathrm{SR}}-1} \Psi(q) x^q e^{-\vartheta_{\mathrm{SR}} x} \tag{7}$$

where $\Psi(q) = ((-1)^q (1 - m_{\mathrm{SR}})_q (\delta_{\mathrm{SR}})^q)/(q!)^2$, $\vartheta_{\mathrm{SR}} = \beta_{\mathrm{SR}} - \delta_{\mathrm{SR}}$, and $(\cdot)_q$ denotes the Pochhammer symbol [33, eq. (p.xliii)]. According to the Alamouti coding with multiple receive antennas, the effective channel gain between satellite and relay is expressed as $\|\mathbf{H}\|_{\mathrm{F}}^2$; therefore, the PDF and CDF are, respectively, obtained as [9]

$$f_{\|\mathbf{H}\|_{\mathrm{F}}^2}(x) = \sum_{q_1=0}^{m_{\mathrm{SR}}-1}, \ldots, \sum_{q_{2N_{\mathrm{R}}}=0}^{m_{\mathrm{SR}}-1} \varphi x^{\Lambda-1} e^{-\vartheta_{\mathrm{SR}} x} \tag{8}$$

$$F_{\|\mathbf{H}\|_{\mathrm{F}}^2}(x) = 1 - \sum_{q_1=0}^{m_{\mathrm{SR}}-1}, \ldots, \sum_{q_{2N_{\mathrm{R}}}=0}^{m_{\mathrm{SR}}-1} \sum_{t_1=0}^{\Lambda-1} \frac{\varphi(\Lambda-1)! x^{t_1} e^{-\vartheta_{\mathrm{SR}} x}}{t_1! (\vartheta_{\mathrm{SR}})^{\Lambda - t_1}} \tag{9}$$

where $\varphi = \prod_{t_2=1}^{2N_{\mathrm{R}}} \Psi(q_{t_2}) \alpha_{\mathrm{SR}}^{2N_{\mathrm{R}}} \prod_{t_3=1}^{2N_{\mathrm{R}}-1} B(\sum_{t_4=1}^{t_3} q_{t_4} + t_3, q_{t_3+1} + 1)$, $\Lambda = (\sum_{j=1}^{2N_{\mathrm{R}}} q_j) + 2N_{\mathrm{R}}$, and $B(\cdot,\cdot)$ represents the Beta function given by [33, eq. (8.384.1)].

2) Terrestrial Channel Statistics: Because we assume that the second hop is exposed to Nakagami-m fading, the PDF and CDF of any squared channel gain between the relay and any antenna ($1 \leq r \leq N$) of the kth user can be represented, respectively, as [34]

$$f_{|h_{k,r}|^2}(x) = \left(\frac{m_k}{\Omega_k}\right)^{m_k} \frac{x^{m_k}}{\Gamma(m_k)} e^{-x\frac{m_k}{\Omega_k}}$$

$$F_{|h_{k,r}|^2}(x) = 1 - e^{-x\frac{m_k}{\Omega_k}} \sum_{n_1=0}^{m_k-1} \frac{(x m_k/\Omega_k)^{n_1}}{n_1!}. \tag{10}$$

[2]Note that the Doppler effect caused by the velocity of the satellite is neglected in the analysis since the GEO satellite is considered. However, the conducted theoretical analyses are also valid for the case of non-GEO satellites, i.e., low-Earth orbit, if the Doppler effect is compensated at the satellite and/or ground user by proper methods [35].

The average power of any link R-U$_k$ is obtained by $\Omega_k = E[|h_{k,r}|^2] = d_k^{-\eta}$, where d_k, η, and m_k represent the normalized distance, path-loss exponent, and Nakagami-m channel parameter of link R-U$_k$, respectively. In addition, because we apply the RAS technique to users, the CDF and PDF corresponding to the squared channel gain between the relay and selected antenna of the kth user are obtained as [38]

$$F_{|\tilde{h}_k|^2}(x) = \left[F_{|h_{k,r}|^2}(x)\right]^N$$

$$f_{|\tilde{h}_k|^2}(x) = N f_{|h_{k,r}|^2}(x) \left[F_{|h_{k,r}|^2}(x)\right]^{N-1}. \tag{11}$$

Here, to exploit NOMA, we assume that users are ordered according to their effective instantaneous channel gains between the relay and users. Thus, in the training period, each user sends the estimated channel gain obtained by the selected receive antenna to the relay sequentially. The relay then sorts them in an ascending order as $|\tilde{h}_1|^2 \leq |\tilde{h}_2|^2 \leq \cdots \leq |\tilde{h}_K|^2$. Next, the relay sends the ordering information to the satellite and users simultaneously. To achieve better user fairness, the satellite is assumed to adjust the power allocation coefficients as $a_1 \geq a_2 \geq \cdots \geq a_K$, where $\sum_{k=1}^{K} a_k = 1$, in the opposite manner to the sorted channel gains. Note that such power ordering is not necessary if the fairness is not a concern [39]

Subsequently, using the PDF expression given in [40] and (11), the PDF of the ordered random variable of $|\tilde{h}_k|^2$ can be expressed as

$$\tilde{f}_{|\tilde{h}_k|^2}(x) = Q_k \sum_{n=0}^{K-k} (-1)^n \binom{K-k}{n} f_{|\tilde{h}_k|^2}(x) \left(F_{|\tilde{h}_k|^2}(x)\right)^{k+n-1}$$

$$= Q_k \sum_{n=0}^{K-k} (-1)^n \binom{K-k}{n} N f_{|h_{k,r}|^2}(x) \left(F_{|h_{k,r}|^2}(x)\right)^{N(k+n)-1} \tag{12}$$

where $Q_k = K!/((K-k)!(K-1)!)$ and $\binom{\cdot}{\cdot}$ denotes the binomial coefficient. If we substitute $f_{|h_{k,r}|^2}(x)$ and $F_{|h_{k,r}|^2}(x)$ given by (10) into (12), we derive the PDF of the ordered random variable $|\tilde{h}_k|^2$ as

$$\tilde{f}_{|\tilde{h}_k|^2}(x) = Q_k \sum_{n=0}^{K-m} (-1)^n \binom{K-m}{n} N \left(\frac{m_k}{\Omega_k}\right)^{m_k} x^{m_k-1}$$

$$e^{-x\frac{m_k}{\Omega_k}} \underbrace{\left(1 - e^{-x\frac{m_k}{\Omega_k}} \sum_{n_1=0}^{m_k-1} \frac{1}{n_1!} \left(x\frac{m_k}{\Omega_k}\right)^{n_1}\right)^{N(k+n)-1}}_{\xi}. \tag{13}$$

If we obtain the closed form of ξ using the power series method [33, eq. (0.314)] in addition with binomial expansion [33, eq. (1.111)], (13) can be rewritten as

$$\tilde{f}_{|\tilde{h}_k|^2}(x) = Q_k \sum_{n=0}^{K-k} \sum_{n_2=0}^{N(k+n)-1} \sum_{n_1=0}^{n_2(m_k-1)} \binom{K-k}{n}$$

$$\binom{N(k+n)-1}{n_2} \frac{N(-1)^{n+n_2}}{\Gamma(m_k)} \left(\frac{m_k}{\Omega_k}\right)^{m_k}$$

$$\mu_{n_1}(n_2, m_k) x^{m_k+n_1-1} e^{-x\frac{m_k}{\Omega_k}(n_2+1)} \tag{14}$$

where $\mu_{n_1}(n_2, m_k)$ represents the multinomial coefficient subjected to $n_1 \geq 0$ [41].

Authorized licensed use limited to: VILLANOVA UNIVERSITY. Downloaded on September 28,2023 at 20:22:30 UTC from IEEE Xplore. Restrictions apply.

III. Performance Analysis of HSTRN With Alamouti-NOMA

A. E2E SINR

Since we have taken the imperfect SIC process into account, without loss of generality, we assume that the SIC error corresponding to the decoding of the jth user's signal by the lth user ($1 \le l \le j-1$) is modeled as $\mathcal{CN}(0, \sigma_{\text{sic}}^2)$ [42], [43]. Here, $\sigma_{\text{sic}}^2 = 1$ and $\sigma_{\text{sic}}^2 = 0$ represent the cases of no SIC and full SIC error, respectively, where $0 \le \sigma_{\text{sic}}^2 \le 1$. Subsequently, with the aid of the Alamouti decoding process as reported in [44], the E2E instantaneous signal-to-interference-plus-noise ratio (SINR) for the kth user (with higher channel gain) to detect the signal of the jth user (with lower channel gain) ($j \le k$) can be expressed with the aid of (4) and (5) as in (15), shown at the bottom of the page.[3] In (15), $\bar{\gamma}_{\text{SR}} = P_{\text{S}}/\sigma_{\text{R}}^2$ and $\bar{\gamma}_k = P_{\text{R}}/\sigma_k^2$ represent the average transmit SNRs of the S–R and R–U$_k$ links, respectively. In addition, $\epsilon_j = \sum_{i=j+1}^{K} a_i$ and $\tilde{\epsilon}_j = \sum_{l=1}^{j-1} a_l \sigma_{\text{sic}}^2$ terms denote the interference and error propagation caused by the imperfect SIC corresponding to the stronger and weaker users.

B. Outage Probability Analysis

OP is a crucial performance metric that provides an insight into the reliability of wireless networks exposed to heavy fading. The OP can be defined as the probability that the E2E instantaneous SINR falls below a certain threshold value. Given the NOMA principle with the SIC technique, the OP of the kth user is defined as the kth user erroneously decoding the jth user's ($1 \le j \le k$) or its own signal; it is expressed as

$$P_k^{\text{out}} = 1 - \mathbb{P}\left(\left\{\gamma_{\text{SRU}_{1\to k}} \ge \gamma_{\text{th},1}\right\} \cap \cdots \cap \left\{\gamma_{\text{SRU}_{k\to k}} \ge \gamma_{\text{th},k}\right\}\right) \tag{16}$$

where the event $\{\gamma_{\text{SRU}_{j\to k}} \ge \gamma_{\text{th},j}\}$ indicates that the jth user's signal can be decoded by the kth user, where $\gamma_{\text{th},j}$ is the threshold SINR intended for the jth user. First, we should examine the event $\{\gamma_{\text{SRU}_{j\to k}} \ge \gamma_{\text{th},j}\}$ which can be represented using (15) as

$$\begin{aligned}
&\left\{\gamma_{\text{SRU}_{j\to k}} \ge \gamma_{\text{th},j}\right\} \\
&= \left\{ \left(|\tilde{h}_k|^2 - \frac{2\gamma_{\text{th},j}}{\bar{\gamma}_k\left(a_j - \gamma_{\text{th},j}\left(\epsilon_j + \tilde{\epsilon}_j\right)\right)} \right) \mathcal{H}\|\mathbf{H}\|_{\text{F}}^2 \right. \\
&\qquad \left. \ge \frac{2\left(\bar{\gamma}_k|\tilde{h}_k|^2 + 1\right)\gamma_{\text{th},j}}{\bar{\gamma}_{\text{SR}}\bar{\gamma}_k\left(a_j - \gamma_{\text{th},j}\left(\epsilon_j + \tilde{\epsilon}_j\right)\right)} \right\} \\
&= \left\{ \|\mathbf{H}\|_{\text{F}}^2 \ge \frac{2\left(\bar{\gamma}_k|\tilde{h}_k|^2 + 1\right)\Delta_j}{\mathcal{H}\bar{\gamma}_{\text{SR}}\left(|\tilde{h}_k|^2 - 2\Delta_j\right)},\ |\tilde{h}_k|^2 > 2\Delta_j \right\}
\end{aligned} \tag{17}$$

[3]It is noted that the users are assumed to be sorted in the ascending order of the effective channel gains.

where the definition $\Delta_j \triangleq (\gamma_{\text{th},j}/[\bar{\gamma}_k(a_j - \gamma_{\text{th},j}(\epsilon_j + \tilde{\epsilon}_j))])$ is made for simplicity in terms of mathematical representations. Afterward, we can represent the OP of the kth user by substituting (17) into the OP definition of P_k^{out} given in (16) as

$$P_k^{\text{out}} = 1 - \mathbb{P}\left(\|\mathbf{H}\|_{\text{F}}^2 \ge \frac{2\left(\bar{\gamma}_k|\tilde{h}_k|^2 + 1\right)\Delta_k^*}{\mathcal{H}\bar{\gamma}_{\text{SR}}\left(|\tilde{h}_k|^2 - 2\Delta_k^*\right)},\ |\tilde{h}_k|^2 > 2\Delta_k^* \right) \tag{18}$$

where $\Delta_k^* = \max_{1\le j\le k}\{\Delta_1, \Delta_2, \ldots, \Delta_j\}$. Note that (18) is valid under the condition that $a_j - \gamma_{\text{th},j}(\epsilon_j + \tilde{\epsilon}_j) > 0$; otherwise, the OP yields 1. Subsequently, we derive the exact OP of the kth user in the closed form in Theorem 1.

Theorem 1: The exact OP of the kth NOMA user is derived as

$$\begin{aligned}
P_k^{\text{out}} = 1 - Q_k \sum_{q} \sum_{n_3=0}^{t_1} \sum_{n_4=0}^{m_k+n_3+n_1-1} & \varphi \binom{K-k}{n} \binom{N(k+n)-1}{n_2} \\
& \binom{t_1}{n_3} \binom{m_k+n_3+n_1-1}{n_4} \frac{(\Lambda-1)!N(-1)^{n+n_2}}{t_1!(\vartheta_{\text{SR}})^{\Lambda-t_1}\Gamma(m_k)} \\
& \left(\frac{2\Delta_k^*}{\mathcal{H}\bar{\gamma}_{\text{SR}}}\right)^{t_1} \left(\frac{m_k}{\Omega_k}\right)^{m_k} \mu_{n_1}(n_2, m_k)(\bar{\gamma}_k)^{n_3} \\
& \left(2\Delta_k^*\right)^{m_k+n_3+n_1-n_4-1} e^{-\vartheta_{\text{SR}}\frac{2\Delta_k^*\bar{\gamma}_k}{\mathcal{H}\bar{\gamma}_{\text{SR}}} - 2\Delta_k^*\left(\frac{m_k}{\Omega_k}\right)(n_2+1)} \\
& 2\left(\frac{2\Delta_k^*\left(2\Delta_k^*\bar{\gamma}_k + 1\right)\vartheta_{\text{SR}}\Omega_k}{\mathcal{H}\bar{\gamma}_{\text{SR}}m_k(n_2+1)}\right)^{\frac{n_4-t_1+1}{2}} \\
& \mathcal{K}_{n_4-t_1+1}\left(2\sqrt{\frac{2\Delta_k^*\left(2\Delta_k^*\bar{\gamma}_k + 1\right)\vartheta_{\text{SR}}m_k(n_2+1)}{\mathcal{H}\bar{\gamma}_{\text{SR}}\Omega_k}}\right)
\end{aligned} \tag{19}$$

where $\mathcal{K}_v(\cdot)$ denotes the vth-order modified Bessel function of the second kind [33, eq. (8.407.1)], and $\sum_q$ represents the summation of multiple variables, defined as

$$\sum_{q} \triangleq \sum_{q_1=0}^{m_{\text{SR}}-1}, \ldots \sum_{q_{2N_{\text{R}}}=0}^{m_{\text{SR}}-1} \sum_{t_1=0}^{\Lambda-1} \sum_{n=0}^{K-k} \sum_{n_2=0}^{N(k+n)-1} \sum_{n_1=0}^{n_2(m_k-1)}. \tag{20}$$

Proof: See Appendix A. ∎

Although the OP expression given by (19) is the exact closed form, it does not provide considerable insight into performance behavior due to its complicated form. Therefore, we investigate the obtained OP asymptotically to gain a better understanding of benefits of Alamouti-NOMA-based HSRTN in the following section.

C. Asymptotic Analysis

In this section, to obtain further insights into the diversity order and array gain, we consider the high SNR approximation given by [45] to observe the performance behavior in the

$$\gamma_{\text{SRU}_{j\to k}} = \frac{\frac{\bar{\gamma}_{\text{SR}}}{2}\bar{\gamma}_k\mathcal{H}\|\mathbf{H}\|_{\text{F}}^2|\tilde{h}_k|^2 a_j}{\frac{\bar{\gamma}_{\text{SR}}}{2}\bar{\gamma}_k\mathcal{H}\|\mathbf{H}\|_{\text{F}}^2|\tilde{h}_k|^2\left(\epsilon_j + \tilde{\epsilon}_j\right) + \bar{\gamma}_{\text{SR}}\mathcal{H}\|\mathbf{H}\|_{\text{F}}^2 + \bar{\gamma}_k|\tilde{h}_k|^2 + 1} \tag{15}$$

Authorized licensed use limited to: VILLANOVA UNIVERSITY. Downloaded on September 28,2023 at 20:22:30 UTC from IEEE Xplore. Restrictions apply.

asymptotic regime. First, we express (18) in a simple form. Thus, by upper bounding the SINR given by (15) with the aid of the harmonic mean property and applying some algebraic manipulations, we obtain the asymptotic OP of the kth user mathematically as

$$P_k^{\text{out},\infty} \approx 1 - \mathbb{P}\left(\min\left(\mathcal{H}\bar{\gamma}\|\mathbf{H}\|_{\mathsf{F}}^2, \bar{\gamma}|\tilde{h}_k|^2\right) \geq 2\Delta_k^*\bar{\gamma}\right) \approx F_{\|\mathbf{H}\|_{\mathsf{F}}^2}^{\infty}\left(\frac{2\zeta_k^*}{\mathcal{H}\bar{\gamma}}\right) + \tilde{F}_{|\tilde{h}_k|^2}^{\infty}\left(\frac{2\zeta_k^*}{\bar{\gamma}}\right) \tag{21}$$

where we use the new definitions as $\zeta_k^* = \max_{1\leq j\leq k}\{\zeta_1, \zeta_2, \ldots, \zeta_j\}$ and $\zeta_j \triangleq (\gamma_{\text{th},j}/[(a_j - \gamma_{\text{th},j}(\epsilon_j + \tilde{\epsilon}_j))])$. In addition, we assume that $\bar{\gamma}_{\text{SR}} = \bar{\gamma}_k = \bar{\gamma}$ for simplicity. By following the method reported in [45], we can express (21) in the form $P_k^{\text{out},\infty} = (G_{\text{a}}\bar{\gamma})^{-G_{\text{d}}} + O(\bar{\gamma}^{-G_{\text{d}}})$, where G_{a} and G_{d} denote the array gain and diversity order, respectively; $O(\cdot)$ represents the omitted higher order terms. Theorem 2 provides the diversity order and array gain of the proposed system.

Theorem 2: The diversity order and array gain that correspond to the kth user are expressed as

$$G_{\text{d}} = \min\{2N_{\text{R}}, m_k \times N \times k\}$$
$$G_{\text{a}} = \begin{cases} \Theta_1, & m_k \times N \times k > 2N_{\text{R}} \\ \Theta_2, & m_k \times N \times k < 2N_{\text{R}} \\ \left(\Theta_1^{-G_{\text{d}}} + \Theta_2^{-G_{\text{d}}}\right)^{-\frac{1}{G_{\text{d}}}}, & m_k \times N \times k = 2N_{\text{R}} \end{cases} \tag{22}$$

where

$$\Theta_1 = \frac{(2N_{\text{R}}!)^{\frac{1}{2N_{\text{R}}}}\mathcal{H}}{\alpha_{\text{SR}}2\zeta_k^*} \text{ and } \Theta_2 = \frac{\binom{K}{k}^{-\frac{1}{m_k N k}}\Omega_k}{\Gamma(m_k+1)^{-\frac{1}{m_k}}2\zeta_k^* m_k}.$$

Proof: See Appendix B. ∎

Remark 1: In the above theorem, the value $2N_{\text{R}}$ in (22) is obtained from Alamouti coding and multiple receive antennas of the relay as a diversity effect since $2N_{\text{R}}$ antennas are used for broadcasting at the satellite and receiving at the relay. Here, it can be seen that the diversity order depends not only on the antenna configuration in the first hop but also on the channel fading (m_k), the number of receiver antennas (N) at users, and user order (k) in the NOMA cluster in the second hop. Furthermore, if the diversity order is limited by the second hop, i.e., $G_{\text{d}} = m_k \times N \times k < 2N_{\text{R}}$, the shadowing conditions in the first hop do not affect the array gain and vice versa when $m_k \times N \times k > 2N_{\text{R}} = G_{\text{d}}$. However, both hops affect the array gain if $m_k \times N \times k = 2N_{\text{R}}$.

IV. Numerical Results

In this section, we verify the theoretical results using Monte Carlo simulations. The parameters for shadowed-Rician channel environments and satellite–terrestrial radio propagation are provided in Tables I and II, respectively. We consider a NOMA-based HSTRN network with three IoT users ($K = 3$) as an example. In all figures, the markers and lines indicate the simulation and analytical results, unless otherwise stated. The parameters for related users are set as $a_1 = 0.6$, $a_2 = 0.3$, and $a_3 = 0.1$ for the allocated power coefficients; $\gamma_{\text{th},1} = 0.4$, $\gamma_{\text{th},2} = 0.8$, and $\gamma_{\text{th},3} = 1.2$ for the threshold SINRs; and

TABLE I
Shadowed-Rician Channel Parameters [36]

Shadowing	$\mathbf{b_{SR}}$	$\mathbf{m_{SR}}$	$\mathbf{\Omega_{SR}}$
Light shadowing	0.158	20	1.29
Average shadowing	0.126	10	0.835
Heavy shadowing	0.063	1	8.97×10^{-4}

TABLE II
Satellite Radio Propagation Parameters [31]

Parameters	Values
Carrier frequency	2 GHz
Carrier bandwidth	15 MHz
Distance between the satellite and relay	35786 km
Antenna gain of the satellite	48 dB
Maximum beam gain at the relay	4 dB
Angle between the beam center and relay	0.2°
One-sided half-power beamwidth	0.4011°
Boltzmann constant	1.38×10^{-23} J/K
Noise temperature at relay	500° K
Scintillation loss	2.2 dB
Atmospheric loss	0.1 dB

$d_1 = 1, d_2 = 0.9$, and $d_3 = 0.8$ for the normalized distances between the relay and users. In addition, the path-loss exponent is set as $\eta = 3$ considering that the users are located in an urban area, while we assume Nakagami-m channel in terrestrial links with parameters $m_1 = m_2 = m_3 = m$ for simplicity. Unless otherwise stated, N_{S} indicates the number of antennas at the satellite while single-antenna relay and perfect SIC are considered in the figures.

Fig. 2 illustrates the OP performance comparisons of the proposed scheme (Alamouti/RAS) that comprises the $N_{\text{S}} = 2$; $N = 3$ antenna configuration and the benchmark single-antenna scenario ($N_{\text{S}} = 1; N = 1$) for (a) heavy shadowing, (b) average shadowing, and (c) light shadowing. The Nakagami-m channel parameter is set as $m = 1$ to observe the performance behavior in the worst terrestrial channel environment. As seen in the figure, numerical results match well with the presented theoretical analysis, which are also supported by the asymptotic (Asymp) curves. It is worth noting that the asymptotic curves match well with the theoretical ones, especially, at high SNR values, although there are gaps at low SNR values in some cases. This mainly comes from a high SNR approximation in our analysis to make it more tractable. Therefore, the occurrence of gaps between the asymptotic curves and exact ones is reasonable at low SNR values.

It is observed that the proposed scheme significantly improves the OP performance of each user under all the different satellite channel environments (heavy, average, and light shadowing) when compared with the benchmark single-antenna scheme. To be more specific, when OP $= 10^{-3}$ for the weak user (U_1), an approximately 14-dB SNR gain can be achieved under heavy shadowing, and the gain is approximately 16 and 18 dB under average and light shadowing, respectively. However, for U_2 and U_3, more SNR gain can be achieved under heavy shadowing effects than under average and light shadowing. The reason for this result is that U_2 and U_3 have better channel qualities than U_1 by assumption. Further, in the case of only the benchmark scheme, we observe that the OP performance of U_1 approaches that of

Authorized licensed use limited to: VILLANOVA UNIVERSITY. Downloaded on September 28,2023 at 20:22:30 UTC from IEEE Xplore. Restrictions apply.

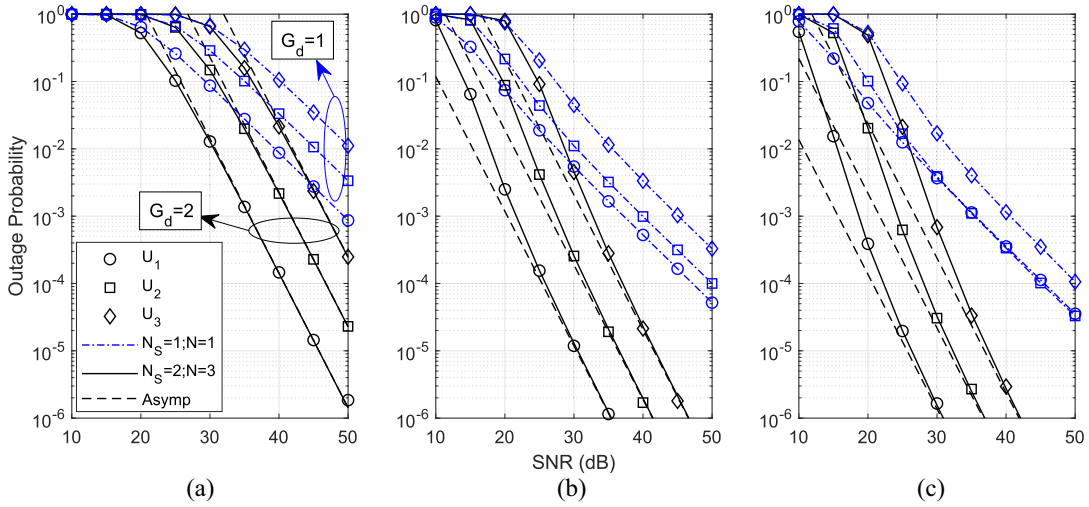

Fig. 2. Outage performance comparisons of the proposed (black curves) and benchmark (blue curves) schemes for (a) heavy shadowing, (b) average shadowing, and (c) light shadowing cases.

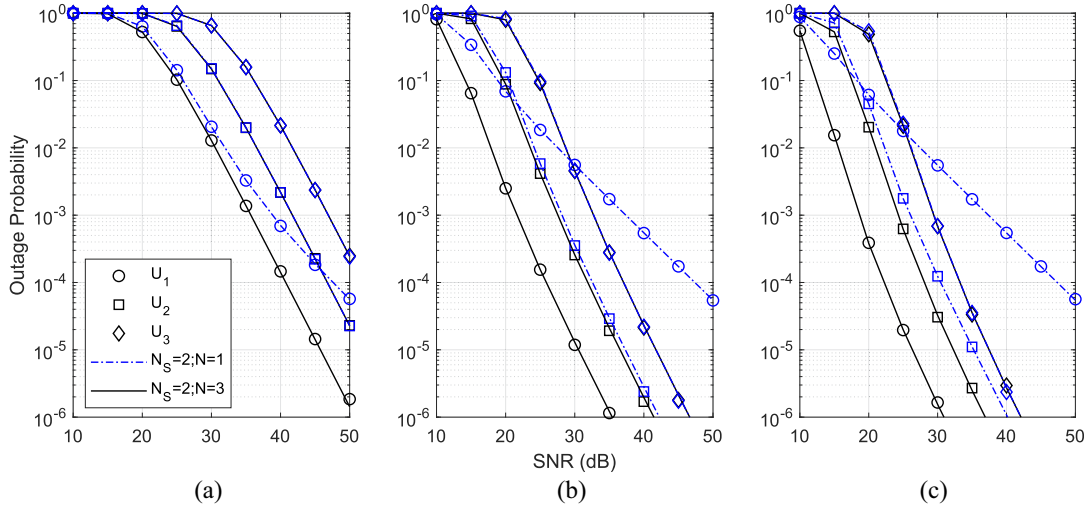

Fig. 3. Outage performance of the proposed scheme (Alamouti/RAS) in case of different number of antennas for (a) heavy shadowing, (b) average shadowing, and (c) light shadowing cases.

U_2 and U_3 under both average and light shadowing effects; even it is the same with U_2 at high SNR values under light shadowing. Moreover, as clearly observed in the figure, with the proposed scheme under the determined configurations, all users exhibit a diversity order of 2 in the high SNR regime, which has also been verified by asymptotic analysis.

In Fig. 3, the OP of the proposed scheme is depicted for (a) heavy shadowing, (b) average shadowing, and (c) light shadowing effects for different numbers of receive antennas and $m = 1$ to investigate the effect of the RAS scheme. We observe that as the number of receive antennas increases, the OP performance of the weakest user (U_1) can be significantly improved such that 8, 22, and 26 dB SNR gains can be obtained for OP$= 10^{-4}$ for heavy, average, and light shadowing effects, respectively. However, for the second user (U_2), a performance improvement can be achieved only in the case of average shadowing and light shadowing effects, i.e., 1 and 2 dB SNR gains, respectively. On the other hand, the strongest user (U_3) cannot enjoy the benefits of the receive diversity under all shadowing cases. This result is also proven by asymptotic analysis such that the diversity order is $G_\mathrm{d} = 2$ for U_3 in both antenna configurations under the determined parameters. Therefore, the first hop has the greatest effect on performance with the array gain $G_\mathrm{a} = (\sqrt{2}\mathcal{H}/\alpha_{\mathrm{SR}} 2\zeta_k^*)$.

Fig. 4 presents the OP performance of the proposed scheme for different number of receive antennas at relay for $m = 1$ and $(N_\mathrm{S} = 2; N = 2)$ to demonstrate the effect of using multiple antennas at the relay. As seen in the figure, OP performances of all users can be significantly improved by increasing number of antennas at the relay. For example, for OP$= 10^{-4}$, all users enjoy an approximately 12-dB SNR gain improvement. When we compare the cases $(N_\mathrm{S} = 2; N_\mathrm{R} = 2; N = 2)$ and $(N_\mathrm{S} = 2; N_\mathrm{R} = 1; N = 2)$, U_2 and U_3 take advantage of diversity order owing to the multiple antennas at relay, such that diversity order is $G_\mathrm{d} = 4$. In contrast, the diversity order of the weakest user (U_1) remains $G_\mathrm{d} = 2$, which is the same as in the case of $(N_\mathrm{S} = 2; N_\mathrm{R} = 1; N = 2)$. However, the array gain of U_1 is affected by only the channel conditions of the second hop while both the first and second hops for

Authorized licensed use limited to: VILLANOVA UNIVERSITY. Downloaded on September 28,2023 at 20:22:30 UTC from IEEE Xplore. Restrictions apply.

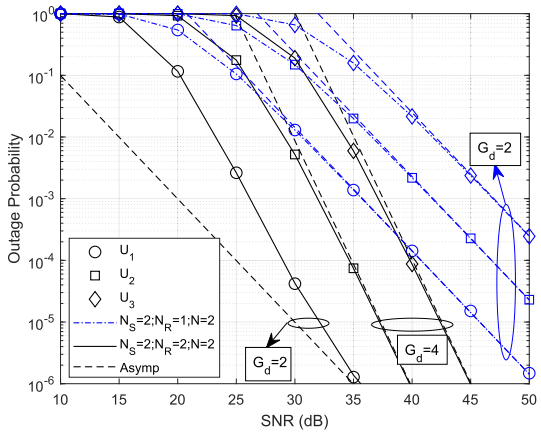

Fig. 4. Outage performance of the proposed scheme for different number of antennas at relay under heavy shadowing.

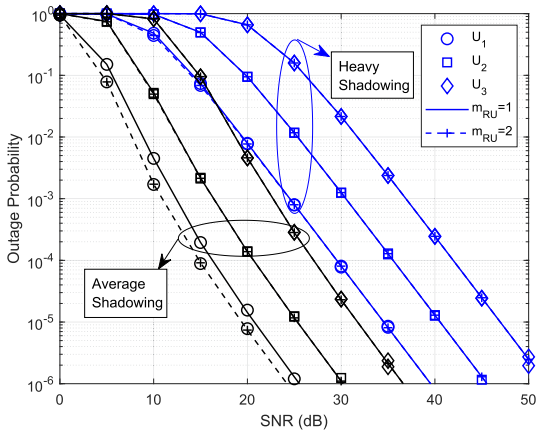

Fig. 6. Outage performance of the proposed scheme for different values of Nakagami-m parameter m with heavy and average shadowing effects.

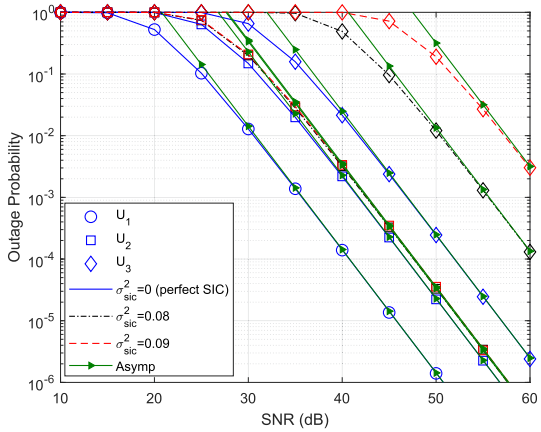

Fig. 5. Outage performance of the proposed scheme in the case of imperfect SIC.

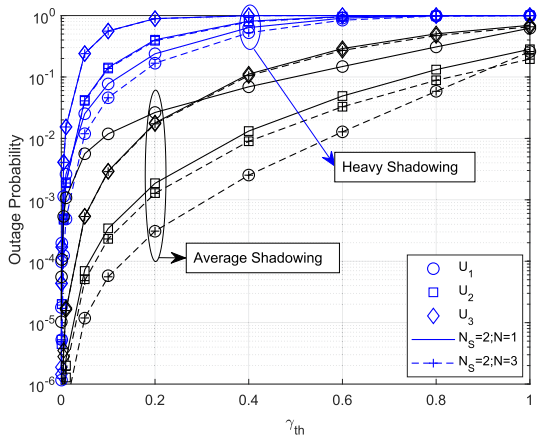

Fig. 7. Outage performance of the proposed scheme versus different values of threshold SINR γ_{th} for heavy and average shadowing effects.

($N_{\text{S}} = 2; N_{\text{R}} = 1; N = 2$). These observations are verified by asymptotic curves obtained through asymptotic analysis.

Fig. 5 illustrates the OP performance of the proposed scheme for different imperfect SIC parameters under heavy shadowing effects. The curves are obtained for $m = 1$ and $N_{\text{S}} = 2; N = 3$. For the OP, the effective range of the SIC error can be obtained as $\sigma^2_{\text{sic}} < 0.0926$ because of the condition $a_j - \gamma_{\text{th},j}(\epsilon_j + \tilde{\epsilon}_j) > 0$ for predefined system parameters. As observed in the figure, imperfect SIC does not affect the performance of U_1 (the weakest user) because no SIC is required. However, the performances of U_2 and U_3 become worse because SIC error increases. In particular, U_3 suffers from the highest performance degradation because the error propagation effect results in SIC errors while decoding the signals of U_1 and U_2. In addition, imperfect SIC does not affect the diversity order in terms of OP, and this is verified by asymptotic curves obtained by theoretical analysis.

Fig. 6 depicts the OP performance of the proposed scheme for heavy and average shadowing effects for different Nakagami-m terrestrial channel conditions of $m = 1$ and $m = 2$. To obtain the curves, the threshold SINRs and antenna configurations are set as $\gamma_{\text{th},1} = 0.04$; $\gamma_{\text{th},2} = 0.08$; $\gamma_{\text{th},3} = 0.12$ and $N_{\text{S}} = N = 2$, respectively. It is obvious from the figure that none of the users can exhibit performance improvement under the heavy shadowing effect with an improvement in the channel condition (when $m = 1$ and $m = 2$ are compared). The key intuition behind this result is that the first hop has the most effect on the performance subjected to the determined configurations. On the other hand, under average shadowing effect, we observe a performance gain in terms of the weakest user (U_1) owing to the improvement in channel conditions in the second hop. This is because when $m = 1$, both hops are effective on the performance, whereas only the first hop has the most effect when $m = 2$. In addition, based on the results of the second and third users, no performance improvement occurs because only the first hop has the most effect for both channel conditions (indicated by $m = 1$ and $m = 2$ parameters), which is verified by asymptotic analysis.

Fig. 7 shows the OP performance of the proposed scheme versus the different values of threshold SINRs ($\gamma_{\text{th}} = \gamma_{\text{th},1} = \gamma_{\text{th},2} = \gamma_{\text{th},3}$) for heavy and average shadowing effects for a fixed SNR= 20 dB and $m = 1$. As observed in the figure, the performance of all users worsens as the threshold values increase under both shadowing effects and antenna configurations. From heavy shadowing results, at all values of γ_{th}, the $N_{\text{S}} = 2; N = 3$ configuration provides a better performance than the $N_{\text{S}} = 2; N = 1$ in terms of the weakest user. However, we observe the same OP performance in terms of the second and third users since the first hop has dominant effect on the performance. However, from the average shadowing results, a significant performance gain can be achieved as the

Authorized licensed use limited to: VILLANOVA UNIVERSITY. Downloaded on September 28,2023 at 20:22:30 UTC from IEEE Xplore. Restrictions apply.

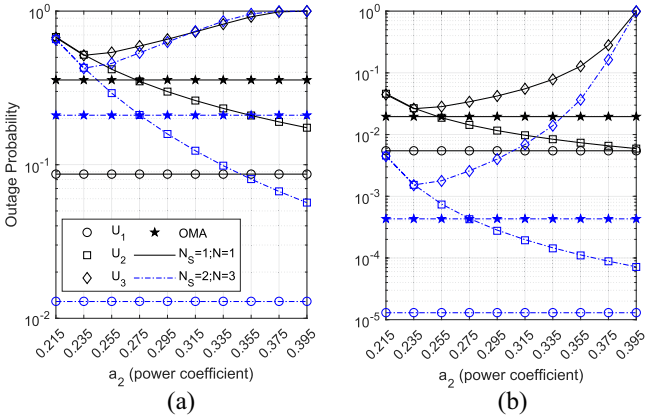

Fig. 8. Outage performance comparisons of the proposed and benchmark schemes versus different values of a_2 for (a) heavy shadowing and (b) average shadowing effects.

threshold values decrease in terms of the weakest user when comparing the $N_S = 2; N = 3$ and $N_S = 2; N = 1$ configurations. Furthermore, we can also observe performance gain in terms of the second and third users such that the gain increases as the threshold values increase.

Fig. 8 depicts the OP performance comparisons of the proposed scheme ($N_S = 2; N = 3$ antenna configuration) and benchmark scheme ($N_S = 1; N = 1$ antenna configuration) versus different power allocation coefficients of U_2 (a_2) for (a) heavy shadowing and (b) average shadowing for a fixed SNR= 30 dB. To obtain the results, we fixed the power level of U_1 as $a_1 = 0.6$ based on $a_1 > (\gamma_{\text{th},1}/\gamma_{\text{th},1} + 1)$ while values range of power levels for U_2 and U_3 are determined by $a_2 > ([(1 - a_1)\gamma_{\text{th},2}]/[\gamma_{\text{th},2} + 1])$ and $a_3 < (1 - a_1/\gamma_{\text{th},2} + 1)$ under the condition of $a_j - \gamma_{\text{th},j} \sum_{i=j+1}^{3} a_i > 0$ defined for (17). Moreover, the proposed scheme is compared with the OMA counterpart subjected to $\log_2(1 + \gamma_{\text{th}}) = \sum_{k=1}^{3} \log_2(1 + \gamma_{\text{th},k})$, where γ_{th} denotes the threshold SNR intended for a single user in the OMA scheme. From the heavy shadowing results, we observe that the OP of U_3 decreases as the power level of U_2 (i.e., a_2) increases, even the OP performance of the proposed scheme approaches that of the benchmark scheme. We can see from this result that the power allocation coefficient for U_3 should be kept at an appropriate level to achieve more performance gain for the proposed scheme. However, for U_2, the performance gap between the proposed and benchmark schemes increases with an increase in the power level related to U_2. In addition, the proposed NOMA scheme outperforms the OMA counterpart at all values of a_2 in terms of the weakest user (U_1). However, in terms of U_2, power allocation coefficient a_2 should be kept above 0.275. Unfortunately, the OMA scheme outperforms the proposed NOMA scheme in terms of U_3 at all values of a_2 for the fixed a_1.[4] Furthermore, similar results are observed for the average shadowing effects.

V. Conclusion

In this article, we propose the use of Alamouti coding and RAS scheme at the satellite and IoT user terminals in a multiuser NOMA-based HSTRN to overcome the CSI burden in the satellite link while ensuring the benefits of spatial diversity. The exact closed-form OP expression for all users is derived to evaluate the performance of the proposed scheme. Furthermore, diversity order and array gain are derived via a high SNR approximation to gain more insight into the OP. The proposed scheme is compared with single-antenna benchmark schemes and the OMA. We observe that the proposed scheme significantly improves the OP of each user under all shadowing environments.

The highest SNR gain is achieved under light shadowing for the weakest user (U_1) and under heavy shadowing for the stronger users (U_2 and U_3). With the RAS, the weakest user enjoys diversity order and array gain under all shadowing effects. On the other hand, the second user utilizes the benefits of spatial diversity only under average and light shadowing, whereas the strongest user cannot achieve any performance improvement, which is also proved through asymptotic analysis. The imperfect SIC severely deteriorates the performance of U_3 more than U_2 because U_3 suffers from the error propagation effect caused by the erroneously decoding the signals of U_1 and U_2. Moreover, the improvement in channel conditions in terrestrial links does not have an impact on the performance of any user under heavy shadowing since the first hop is more effective. Furthermore, the proposed NOMA scheme outperforms OMA for the weakest user at all power levels allocated to the second user, while power level should be kept above a certain threshold for the second user. We observed that channels in the satellite link have a greater effect on the performance, and it can also change performance behavior. Therefore, we consider addressing the imperfections that occurred in satellite and terrestrial links in our future research.

Appendix A
Proof of Theorem 1

The OP of the kth user given in (18) can be expressed mathematically using the fundamental probability theorem as follows:

$$P_k^{\text{out}} = 1 - \int_{y=2\Delta_k^*}^{\infty} \int_{x=\frac{2(\bar{\gamma}_k y+1)\Delta_k^*}{\mathcal{H}\bar{\gamma}_{\text{SR}}(y-2\Delta_k^*)}}^{\infty} f_{\|\mathbf{H}\|_{\text{F}}^2}(x) \tilde{f}_{|\tilde{h}_k|^2}(y) dx dy$$
$$= \tilde{F}_{|\tilde{h}_k|^2}(2\Delta_k^*) + \int_{y=2\Delta_k^*}^{\infty} F_{\|\mathbf{H}\|_{\text{F}}^2}\left(\frac{2(\bar{\gamma}_k y+1)\Delta_k^*}{\mathcal{H}\bar{\gamma}_{\text{SR}}(y-2\Delta_k^*)}\right) \tilde{f}_{|\tilde{h}_k|^2}(y) dy. \quad (23)$$

In (23), $\tilde{f}_X(x)$ and $\tilde{F}_X(x)$ represent the PDF and CDF of the ordered random variable X, respectively. Thus, if we substitute (9) and (14) into (23), we obtain

$$P_k^{\text{out}} = 1 - Q_k \sum_{q} \varphi \binom{K-k}{n} \binom{N(k+n)-1}{n_2} \frac{(\Lambda-1)!\left(2\Delta_k^*/(\mathcal{H}\bar{\gamma}_{\text{SR}})\right)^{t_1}}{t_1!(\vartheta_{\text{SR}})^{\Lambda-t_1}} \frac{N(-1)^{n+n_2}}{\Gamma(m_k)} \left(\frac{m_k}{\Omega_k}\right)^{m_k} \mu_{n_1}(n_2, m_k) \int_{y=2\Delta_k*}^{\infty} \left(\frac{\bar{\gamma}_k y+1}{y-2\Delta_k^*}\right)^{t_1} y^{m_k+n_1-1} e^{-\vartheta_{\text{SR}}\left(\frac{2(\bar{\gamma}_k y+1)\Delta_k^*}{\mathcal{H}\bar{\gamma}_{\text{SR}}(y-2\Delta_k^*)}\right)} e^{-y\left(\frac{m_k}{\Omega_k}\right)(n_2+1)} dy. \quad (24)$$

[4]To tackle this issue, the optimal power allocation for NOMA needs to be taken into account; however, it is beyond the scope of this article and is a topic of a further study.

Authorized licensed use limited to: VILLANOVA UNIVERSITY. Downloaded on September 28,2023 at 20:22:30 UTC from IEEE Xplore. Restrictions apply.

Subsequently, using the binomial expansion [33, eq. (1.111)] and closed-form integral solution provided in [33, eq. (3.471.9)], we obtain the OP of the kth user in the closed form as in (19). Thus, the proof is completed.

APPENDIX B
PROOF OF THEOREM 2

By using the Maclaurin series in (8) and omitting the higher order terms, we obtain $e^{-\vartheta_{\mathrm{SR}} 2\zeta_k^*/\mathcal{H}\bar{\gamma}} \approx 1 - \vartheta_{\mathrm{SR}} 2\zeta_k^*/\mathcal{H}\bar{\gamma}$. Because $\bar{\gamma} \to \infty$ implies $-\vartheta_{\mathrm{SR}} 2\zeta_k^*/\mathcal{H}\bar{\gamma} \to 0$, we can obtain $f^{\infty}_{\|\mathbf{H}\|_{\mathrm{F}}^2}(2\zeta_k^*/\mathcal{H}\bar{\gamma}) \approx \varphi(2\zeta_k^*/\mathcal{H}\bar{\gamma})^{\Lambda-1}$. Here, we can show that $\varphi = \alpha_{\mathrm{SR}}^{2N_{\mathrm{R}}}/(2N_{\mathrm{R}}-1)!$ and $\Lambda = 2N_{\mathrm{R}}$. Thus, we obtain $f^{\infty}_{\|\mathbf{H}\|_{\mathrm{F}}^2}(2\zeta_k^*/\mathcal{H}\bar{\gamma}) \approx (\alpha_{\mathrm{SR}}^{2N_{\mathrm{R}}}(2\zeta_k^*/\mathcal{H}\bar{\gamma})^{2N_{\mathrm{R}}-1})/(2N_{\mathrm{R}}-1)!$. Finally, by taking the integral of the obtained PDF, we can express the CDF in (9) asymptotically as

$$F^{\infty}_{\|\mathbf{H}\|_{\mathrm{F}}^2}\left(\frac{2\zeta_k^*}{\mathcal{H}\bar{\gamma}}\right) = \left(\frac{(2N_{\mathrm{R}}!)^{\frac{1}{2N_{\mathrm{R}}}}\mathcal{H}\bar{\gamma}}{\alpha_{\mathrm{SR}} 2\zeta_k^*}\right)^{-2N_{\mathrm{R}}}. \tag{25}$$

Next, to determine the asymptotic CDF of (14), we need to express the CDF of the ordered random variable related to the second hop as $\tilde{F}_{|\tilde{h}_k|^2}(x) = Q_k \sum_{n=0}^{K-k}[(-1)^n/k+n]\binom{K-k}{n}(F_{|\tilde{h}_k|^2}(x))^{k+n}$. For the high SNR regime ($\bar{\gamma} \to \infty$), we consider the lower order terms effective on the value of x; we can then obtain $\tilde{F}^{\infty}_{|\tilde{h}_k|^2}(x) = \binom{K}{k}(F^{\infty}_{|h_{k,r}|^2}(x))^{Nk}$. By using the asymptotic property of incomplete Gamma function provided by [46, eq. (45:9:1)], we can obtain the asymptotic CDF of the random variable between the relay and kth user's any antenna as $F^{\infty}_{|h_{k,r}|^2}(x) = (xm_k/\Omega_k)^{m_k}/\Gamma(m_k+1)$. By substituting $2\zeta_k^*/\bar{\gamma}$ and $F^{\infty}_{|h_{k,r}|^2}(x)$ into $\tilde{F}^{\infty}_{|\tilde{h}_k|^2}(x)$, we can express the CDF of (14) asymptotically as

$$\tilde{F}^{\infty}_{|\tilde{h}_k|^2}\left(\frac{2\zeta_k^*}{\bar{\gamma}}\right) = \left(\frac{\binom{K}{k}^{-\frac{1}{m_k Nk}}}{\Gamma(m_k+1)^{-\frac{1}{m_k}}}\frac{\Omega_k\bar{\gamma}}{2\zeta_k^* m_k}\right)^{-m_k Nk}. \tag{26}$$

By using (25), (26), and $P_k^{\mathrm{out},\infty} = (G_{\mathrm{a}}\bar{\gamma})^{-G_{\mathrm{d}}} + O(\bar{\gamma}^{-G_{\mathrm{d}}})$, we obtain the diversity order and array gain as in (22). Thus, the proof is completed.

REFERENCES

[1] M. Vaezi et al., "Cellular, wide-area, and non-terrestrial IoT: A survey on 5G advances and the road toward 6G," *IEEE Commun. Surveys Tuts.*, vol. 24, no. 2, pp. 1117–1174, 2nd Quart., 2022.

[2] R. G. Gopal and N. B. Ammar, "Framework for unifying 5G and next generation satellite communications," *IEEE Netw.*, vol. 32, no. 5, pp. 16–24, Sep./Oct. 2018.

[3] M. Giordani and M. Zorzi, "Non-terrestrial networks in the 6G era: Challenges and opportunities," *IEEE Netw.*, vol. 35, no. 2, pp. 244–251, Mar./Apr. 2021.

[4] B. Evans et al., "Integration of satellite and terrestrial systems in future multimedia communications," *IEEE Wireless Commun.*, vol. 12, no. 5, pp. 72–80, Oct. 2005.

[5] B. Paillassa, B. Escrig, R. Dhaou, M.-L. Boucheret, and C. Bes, "Improving satellite services with cooperative communications," *Int. J. Satell. Commun. Netw.*, vol. 29, no. 6, pp. 479–500, 2011.

[6] M. R. Bhatnagar and M. K. Arti, "Performance analysis of AF based hybrid satellite–terrestrial cooperative network over generalized fading channels," *IEEE Commun. Lett.*, vol. 17, no. 10, pp. 1912–1915, Oct. 2013.

[7] L. Yang and M. O. Hasna, "Performance analysis of amplify-and-forward hybrid satellite–terrestrial networks with cochannel interference," *IEEE Trans. Commun.*, vol. 63, no. 12, pp. 5052–5061, Dec. 2015.

[8] M. K. Arti and M. R. Bhatnagar, "Beamforming and combining in hybrid satellite–terrestrial cooperative systems," *IEEE Commun. Lett.*, vol. 18, no. 7, pp. 483–486, Mar. 2014.

[9] N. I. Miridakis, D. D. Vergados, and A. Michalas, "Dual-hop communication over a satellite relay and shadowed rician channels," *IEEE Trans. Veh. Technol.*, vol. 64, no. 9, pp. 4031–4040, Sep. 2015.

[10] V. Bankey, P. K. Upadhyay, D. B. Da Costa, P. S. Bithas, A. G. Kanatas, and U. S. Dias, "Performance analysis of multi-antenna multiuser hybrid satellite–terrestrial relay systems for mobile services delivery," *IEEE Access*, vol. 6, pp. 24729–24745, 2018.

[11] P. K. Upadhyay and P. K. Sharma, "Max-max user-relay selection scheme in multiuser and multirelay hybrid satellite–terrestrial relay systems," *IEEE Commun. Lett.*, vol. 20, no. 2, pp. 268–271, Feb. 2016.

[12] J. Jiao, Y. Sun, S. Wu, Y. Wang, and Q. Zhang, "Network utility maximization resource allocation for NOMA in satellite-based Internet of Things," *IEEE Internet Things J.*, vol. 7, no. 4, pp. 3230–3242, Apr. 2020.

[13] J. Chu, X. Chen, C. Zhong, and Z. Zhang, "Robust design for NOMA-based multibeam LEO satellite Internet of Things," *IEEE Internet Things J.*, vol. 8, no. 3, pp. 1959–1970, Feb. 2021.

[14] W. Shin, M. Vaezi, B. Lee, D. J. Love, J. Lee, and H. V. Poor, "Non-orthogonal multiple access in multi-cell networks: Theory, performance, and practical challenges," *IEEE Commun. Mag.*, vol. 55, no. 10, pp. 176–183, Oct. 2017.

[15] Z. Ding et al., "Application of non-orthogonal multiple access in LTE and 5G networks," *IEEE Commun. Mag.*, vol. 55, no. 2, pp. 185–191, Feb. 2017.

[16] M. Aldababsa, M. Toka, S. Gokçeli, G. K. Kurt, and O. Kucur, "A tutorial on non-orthogonal multiple access for 5G and beyond," *Wireless Commun. Mobile Comput.*, vol. 2018, pp. 1–24, Jun. 2018.

[17] X. Zhu, C. Jiang, N. G. Kuang, and J. Lu, "Non-orthogonal multiple access based integrated terrestrial-satellite networks," *IEEE J. Sel. Areas Commun.*, vol. 35, no. 10, pp. 2253–2267, Oct. 2017.

[18] X. Yan, H. Xiao, C. X. Wang, K. An, A. T. Chronopoulos, and G. Zheng, "Performance analysis of NOMA-based land mobile satellite networks," *IEEE Access*, vol. 6, pp. 31327–31339, 2018.

[19] X. Yue et al., "Outage behaviors of NOMA-based satellite network over shadowed-Rician fading channels," *IEEE Trans. Veh. Technol.*, vol. 69, no. 6, pp. 6818–6821, Jun. 2020.

[20] X. Yan, H. Xiao, K. An, G. Zheng, and W. Tao, "Hybrid satellite terrestrial relay networks with cooperative non-orthogonal multiple access," *IEEE Commun. Lett.*, vol. 22, no. 5, pp. 978–981, May 2018.

[21] S. Xie, B. Zhang, D. Guo, and B. Zhao, "Performance analysis and power allocation for NOMA-based hybrid satellite–terrestrial relay networks with imperfect channel state information," *IEEE Access*, vol. 7, pp. 136279–136289, 2019.

[22] V. Singh and P. K. Upadhyay, "Exploiting FD/HD cooperative-NOMA in underlay cognitive hybrid satellite–terrestrial networks," *IEEE Trans. Cogn. Commun. Netw.*, vol. 8, no. 1, pp. 246–262, Mar. 2022.

[23] X. Li, Y. Chen, P. Xue, G. Lv, and M. Shu, "Outage performance for satellite-assisted cooperative NOMA systems with coordinated direct and relay transmission," *IEEE Commun. Lett.*, vol. 24, no. 10, pp. 2285–2289, Oct. 2020.

[24] X. Yan, H. Xiao, C. Wang, and K. An, "Outage performance of NOMA-based hybrid satellite–terrestrial relay networks," *IEEE Wireless Commun. Lett.*, vol. 7, no. 4, pp. 538–541, Aug. 2018.

[25] Y. He, J. Jiao, X. Liang, S. Wu, Y. Wang, and Q. Zhang, "Outage performance of millimeter-wave band NOMA downlink system in satellite-based IoT," in *Proc. IEEE Int. Conf. Commun. China (ICCC)*, Changchun, China, 2019, pp. 256–359.

[26] M. K. Arti and S. K. Jindal, "OSTBC transmission in shadowed-rician land mobile satellite links," *IEEE Trans. Veh. Techol.*, vol. 65, no. 7, pp. 5771–5777, Jul. 2016.

[27] Y. Ruan, Y. Li, R. Zhang, and H. Zhang, "Performance analysis of hybrid satellite–terrestrial cooperative networks with distributed Alamouti code," in *Proc. IEEE Veh. Technol. Conf. (VTC Spring)*, Nanjing, China, 2016, pp. 1–5.

[28] B. Zhao, H. Kong, X. Liu, M. Lin, J. Ouyang, and W.-P. Zhu, "Transmit diversity and performance analysis for aeronautical broadband satellite communication systems," *Phys. Commun.*, vol. 48, no. 5, 2021, Art. no. 101424.

Authorized licensed use limited to: VILLANOVA UNIVERSITY. Downloaded on September 28,2023 at 20:22:30 UTC from IEEE Xplore. Restrictions apply.

[29] S. M. Alamouti, "A simple transmit diversity technique for wireless communications," *IEEE J. Sel. Areas Commun.*, vol. 16, no. 8, pp. 1451–1458, Oct. 1998.
[30] M. Toka and W. Shin, "NOMA based hybrid satellite–terrestrial relay networks," in *Proc. IEEE 6th Int. Conf. Consum. Electron. Asia (ICCE-Asia)*, 2021, pp. 1–3.
[31] "Solutions for NR to support non-terrestrial networks NTN," 3GPP, Sophia Antipolis, France, Rep. TR-38.821, May 2021.
[32] "Calculation of free-space attenuation," Int. Telecommun. Union, Geneva, Switzerland, Rep. ITU-R P.525-4, Aug. 2019.
[33] I. S. Gradshteyn and I. M. Ryzhic, *Table of Integrals, Series, and Products*, 6th ed. New York, NY, USA: Academic, 2000.
[34] M. K. Simon and M. S. Alouini, *Digital Communications Over Fading Channels*, vol. 95, 2nd ed. New York, NY, USA: Wiley, 2005.
[35] J. Ye, G. Pan, and M.-S. Alouini, "Earth rotation-aware non-stationary satellite communication systems: Modeling and analysis," *IEEE Trans. Wireless Commun.*, vol. 20, no. 9, pp. 5942–5956, Sep. 2021.
[36] A. Abdi, W. Lau, M.-S. Alouini, and M. Kaveh, "A new simple model for land mobile satellite channels: First- and second-order statistics," *IEEE Trans. Wireless Commun.*, vol. 2, no. 3, pp. 519–528, May 2003.
[37] G. Alfano and A. De Maio, "Sum of squared Shadowed-Rice random variables and its application to communication systems performance prediction," *IEEE Trans. Wireless Commun.*, vol. 6, no. 10, pp. 3540–3545, Oct. 2007.
[38] H. David and H. Nagaraja, *Order statistics*, 3rd ed. Hoboken, NJ, USA: Wiley, 2003.
[39] M. Vaezi, R. Schober, Z. Ding, and H. V. Poor, "Non-orthogonal multiple access: Common myths and critical questions," *IEEE Wireless Commun.*, vol. 26, no. 5, pp. 174–180, Oct. 2019.
[40] X. Yue, Y. Liu, S. Kang, and A. Nallanathan, "Performance analysis of NOMA with fixed gain relaying over Nakagami-*m* fading channels," *IEEE Access*, vol. 5, pp. 5445–5454, 2015.
[41] M. Toka and O. Kucur, "Non-orthogonal multiple access with Alamouti space–time block coding," *IEEE Commun. Lett.*, vol. 22, no. 9, pp. 9697–9706, Sep. 2018.
[42] J. G. Andrews and T. H. Y. Meng, "Performance of multicarrier CDMA with successive interference cancellation in a multipath fading channel," *IEEE Trans. Commun.*, vol. 52, no. 5, pp. 811–822, May 2004.
[43] D. Tweed, M. Derakhshani, S. Parsaeefard, and T. Le-Ngoc, "Outage-constrained resource allocation in uplink NOMA for critical applications," *IEEE Access*, vol. 5, pp. 27636–27648, 2017.
[44] S. Chen, W. Wang, X. Zhang, and Z. Sun, "Performance analysis of OSTBC transmission in amplify-and-forward cooperative relay networks," *IEEE Trans. Veh. Techol.*, vol. 59, no. 1, pp. 105–113, Jan. 2010.
[45] Z. Wang and G. B. Giannakis, "A simple and general parameterization quantifying performance in fading channels," *IEEE Trans. Commun.*, vol. 51, no. 8, pp. 1389–1398, Aug. 2003.
[46] K. B. Oldham, J. Myland, and J. Spanier, *An Atlas of Functions with Equator the Atlas Function Calculator*, 2nd ed. New York, NY, USA: Springer, 2008.

Mesut Toka (Member, IEEE) received the B.Sc. degree in electrical and electronics engineering from Erciyes University, Kayseri, Turkey, in 2011, the M.Sc. degree in electrical and electronics engineering from Ömer Halisdemir University (OHU), Niğde, Turkey, in 2015, and the Ph.D. degree in electronics engineering from Gebze Technical University (GTU), Darica, Turkey, in 2021.

He was a Research and Teaching Assistant with OHU and GTU during his M.Sc. and Ph.D. periods. He is currently working as a Postdoctoral Researcher of Electrical and Computer Engineering with Ajou University, Suwon, South Korea. His research interests include cooperative communications, diversity techniques, full-duplex communications, multiple access techniques, and satellite–terrestrial relay networks.

Mojtaba Vaezi (Senior Member, IEEE) received the Ph.D. degree in electrical and computer engineering from McGill University, Montreal, QC, Canada, in 2014.

From 2015 to 2018, he was with Princeton University, Princeton, NJ, USA, as a Postdoctoral Research Fellow and an Associate Research Scholar. He is currently an Assistant Professor of ECE with Villanova University, Villanova, PA, USA. Before joining Princeton University, he was a Researcher with Ericsson Research, Montreal. Among his publications in these areas is the book *Multiple Access Techniques for 5G Wireless Networks and Beyond* (Springer, 2019). His research interests include the broad areas of signal processing and machine learning for wireless communications with an emphasis on physical-layer security and fifth generation and beyond radio access technologies.

Dr. Vaezi is a recipient of several academic, leadership, and research awards, including the McGill Engineering Doctoral Award, the IEEE Larry K. Wilson Regional Student Activities Award in 2013, the Natural Sciences and Engineering Research Council of Canada Postdoctoral Fellowship in 2014, the Ministry of Science and ICT of Korea's Best Paper Award in 2017, the IEEE Communications Letters Exemplary Editor Award in 2018, the 2020 IEEE Communications Society Fred W. Ellersick Prize, and the 2021 IEEE Philadelphia Section Delaware Valley Engineer of the Year Award. He is an Editor of the IEEE TRANSACTIONS ON COMMUNICATIONS and an Associate Editor of the IEEE COMMUNICATIONS LETTERS. He also was an Associate Editor of the *IEEE Communications Magazine*. He has co-organized six NOMA workshops at IEEE VTC 2017-Spring, Globecom'17, Globecom'18, and ICC'18, ICC'19, ICC'20.

Wonjae Shin (Senior Member, IEEE) received the B.S. and M.S. degrees from Korea Advanced Institute of Science and Technology, Daejeon, South Korea, in 2005 and 2007, respectively, and the Ph.D. degree from the Department of Electrical and Computer Engineering, Seoul National University (SNU), Seoul, South Korea, in 2017.

From 2007 to 2014, he was a member of the technical staff with the Samsung Advanced Institute of Technology and Samsung Electronics Company Ltd., Suwon, South Korea, where he contributed to next-generation wireless communication networks, especially for 3GPP LTE/LTE-advanced standardizations. From 2016 to 2018, he was a Visiting Scholar and a Postdoctoral Research Fellow with Princeton University, Princeton, NJ, USA. He is currently an Associate Professor with the Department of Electrical and Computer Engineering, Ajou University, Suwon. Prior to joining Ajou University, he was a Faculty Member with Pusan National University, Busan, South Korea, from 2018 to 2021. His research interests include the design and analysis of future wireless communications, such as interference-limited networks and machine learning for wireless networks.

Dr. Shin was the recipient of the Fred W. Ellersick Prize and the Asia–Pacific Outstanding Young Researcher Award from the IEEE Communications Society in 2020, the Best Ph.D. Dissertation Award from SNU in 2017, the Gold Prize from the IEEE Student Paper Contest (Seoul Section) in 2014, and the Award of the Ministry of Science and ICT of Korea in IDIS-Electronic News ICT Paper Contest in 2017. He was a co-recipient of the SAIT Patent Award in 2010, the *Samsung Journal of Innovative Technology* in 2010, the Samsung Human Tech Paper Contest in 2010, and the Samsung CEO Award in 2013. He was recognized as an Exemplary Reviewer by IEEE WIRELESS COMMUNICATIONS LETTERS in 2014 and IEEE TRANSACTIONS ON COMMUNICATIONS in 2019. He was also awarded several fellowships, including the Samsung Fellowship Program in 2014 and the SNU Long-Term Overseas Study Scholarship in 2016. He is an Editor of IEEE OPEN JOURNAL OF COMMUNICATIONS SOCIETY.

Authorized licensed use limited to: VILLANOVA UNIVERSITY. Downloaded on September 28,2023 at 20:22:30 UTC from IEEE Xplore. Restrictions apply.